annalen der physik
www.ann-phys.org

Manipulation of Polarizations with Crystalline Orientation for an Elliptically Polarized Passively Q-Switched Raman Laser

*Yinming An, Haolin Yang, Bohan Lin, Jiaxiang Bi, and Jun Dong**

Polarization control of dual-wavelength high peak power Raman lasers based on passively Q-switched technology and yttrium vanadate (YVO_4) crystal are widely used for generating novel laser sources, terahertz wave, material processing, and manipulating microparticles. However, the Raman lasers are usually linear polarization. Here, elliptical polarizations with controllable ellipticity and azimuthal angle are manipulated by adjusting the crystalline orientation of *a*-cut YVO_4 crystal in a passively Q-switched Raman laser constructed with a Cr^{4+},Nd^{3+}:$Y_3Al_5O_{12}$ (Cr,Nd:YAG) crystal and a a-cut YVO_4 crystal. The ellipticity of the elliptically polarized dual-wavelength Raman laser varies in a sinusoid modulation as *a*-cut YVO_4 crystal rotates with respect to the major axis of the intracavity fundamental laser and increases with applied pump power. The azimuthal angle varies in the same speed as *a*-cut YVO_4 crystal rotates. Anisotropic behavior of sinusoidal modulation of output power, pulse energy, and peak power is observed as *a*-cut YVO_4 crystal rotates. There are four peaks and four troughs for ellipticity, output power, pulse energy, and peak power within a 360° rotation of *a*-cut YVO_4 crystal. This work provides a solid and simple method for developing elliptical polarization controllable dual-wavelength passively Q-switched Raman laser with high peak power for various potential applications.

1. Introduction

Manipulation of the state of polarization (SoP) such as ellipticity and azimuthal angle of the elliptically polarized high peak power laser is essential for applications in various areas such as materials processing,[1] manipulation of molecules,[2,3] optical alignment and spinning of laser-trapped microparticles,[4] high harmonic generation,[5] supercontinuum generation,[6] and terahertz wave generation.[7] High peak power ultrafast fiber lasers with certain polarization have been demonstrated for broadband laser spectrum and multiple wavelength laser oscillation;[8,9] however, the lasers are complicated, pulse energy is low and polarization state is difficult to manipulate. Compared to complicated ultrafast fiber lasers, passively Q-switched Raman lasers are compact, robustness and easy to operate and maintain. Various Raman crystals and saturable absorbers have been used for developing high peak power passively Q-switched Raman laser. Tetragonal vanadate crystals such as yttrium vanadate (YVO_4) and gadolinium vanadate ($GdVO_4$) crystals have been widely used as Raman gain media for expanding laser wavelength.[10] Efficient laser performance of continuous-wave, Q-switched, and mode-locked lasers has been demonstrated based on Nd:YVO_4[11] and Yb:YVO_4[12] crystals. Taking advantage of stimulated Raman scattering (SRS) effect of YVO_4 crystal,[13] multiple wavelength lasers including fundamental and Raman lasers oscillating simultaneously have been developed[14] with actively Q-switching and passively Q-switching technology,[15,16] which have a wide range of applications in the fields of space optical communication,[17] laser sensing,[18] digital holography technology,[19] and nonlinear frequency conversion.[20] In particular, the small-spaced dual-wavelength laser has been used to generate terahertz waves through difference frequency,[21] which have been widely used in human medical imaging and biological detection.[22] Compact eye-safe 1525 nm actively Q-switched Nd:YVO_4 self-Raman laser has been converted from 1342 nm fundamental laser with 890 cm^{-1} Raman shift line.[23] At pump power of 13.5 W, the average output power is 1.2 W and optical conversion efficiency is 8.9%. 1178.9/1199.9 nm dual-wavelength Raman laser was generated in an actively Q-switched Nd:YVO_4/YVO_4 self-Raman laser with 890 cm^{-1} Raman shift line.[24] Compared with Nd:YVO_4 crystal, YVO_4 crystal with perfect lattice structure has high thermal conductivity and laser damage threshold. Raman frequency shift modes of YVO_4 crystal have been studied under a polarized beam pumping from room temperature to 473 K.[25] Performance was dramatically improved in an actively Q-switched Nd:YVO_4/YVO_4

Y. An, H. Yang, J. Bi, Prof. J. Dong
Laboratory of Laser and Applied Photonics (LLAP)
Department of Electronic Engineering
School of Electronic Science and Engineering
Xiamen University
Xiamen 361005, China
E-mail: jdong@xmu.edu.cn
B. Lin
School of Information Science and Technology
Xiamen University Malaysia, Sepang
Selangor Darul Ehsan 43900, Malaysia

The ORCID identification number(s) for the author(s) of this article can be found under https://doi.org/10.1002/andp.202100068

DOI: 10.1002/andp.202100068

Raman laser by using YVO_4 crystal as Raman gain medium.[26] Stable 1164.4/1174.7 nm dual-wavelength Raman laser with equivalent intensity was demonstrated in a directly pumped Nd:$GdVO_4$/Cr^{4+}:YAG/YVO_4 passively Q-switched Raman microchip laser by utilizing 816 and 890 cm^{-1} Raman shift lines of the YVO_4 crystal.[27] With *a*-cut YVO_4 crystal as Raman gain medium and a Nd^{3+}:$Y_3Al_5O_{12}$ (Nd:YAG) crystal as gain medium, linearly polarized Raman laser was generated in an actively Q-switched Nd:YAG Raman laser.[28] Raman laser with linear polarization was generated in a continuous-wave microchip Raman laser constructed with Yb:YAG and Nd:YVO_4 crystals.[29,30] However, the SoP of these dual-wavelength Raman lasers is linear polarized and difficult to manipulate for fulfill various applications. Therefore, control of SoP for the elliptically polarized dual-wavelength Raman laser is a challenge for achieving desired ellipticity and azimuthal angle, sometime control of the chirality of the elliptically polarized laser is required for rotating molecules in biological and medical applications.

Cr^{4+}:YAG crystal has been used as saturable absorber for constructing passively Q-switched Raman lasers. However, the insertion of Cr^{4+}:YAG crystal inside the Raman laser cavity introduces reflection and diffraction losses and makes the passively Q-switched Raman laser less efficient. The crystalline orientation dependent saturable absorption of Cr^{4+}:YAG crystal has great effect on the polarization states of passively Q-switched laser.[31] Thus, the crystalline orientation of Cr^{4+}:YAG crystal has to be carefully aligned with orientation of gain medium to realize elliptical polarization. Cr^{4+},Nd^{3+}:$Y_3Al_5O_{12}$ (Cr,Nd:YAG) crystal as one of self-Q-switched crystals has advantages for maintaining the crystalline orientation matching for Nd^{3+} ions and Cr^{4+} ions, therefore, it is ideal candidate for achieving perfect elliptically polarized laser operation in passively Q-switched laser. High peak power and efficient lasers have been achieved in Cr,Nd:YAG self-Q-switched lasers[32–34] and Cr,Yb:YAG self-Q-switched lasers.[35,36] It is essential to maintain elliptical polarization with fixed azimuthal angle for fundamental laser in passively Q-switched Raman laser to achieve tetrahedral *a*-cut YVO_4 crystalline orientation manipulated polarization states of Raman lasers.

In this paper, we report a new method for realizing flexible control of SoP for elliptically polarized dual-wavelength passively Q-switched Raman laser by rotating *a*-cut YVO_4 crystal, which acts as a Raman gain medium and an output coupler. We demonstrated that the elliptically polarized dual-wavelength Raman lasers with desired ellipticity and azimuthal angle have realized by rotating the *a*-cut YVO_4 crystal and changing applied pump power. The sinusoidal variation of the average output power, pulse energy, and peak power of passively Q-switched dual-wavelength Raman laser has been observed by rotating *a*-cut YVO_4 crystal with respect to the major axis of the elliptically polarized intracavity fundamental laser.

2. Experimental Section

The schematic for manipulating polarization state of elliptically polarized dual-wavelength Raman laser generated in a self-Q-switched Raman laser by rotating *a*-cut YVO_4 crystal is shown in **Figure 1**a. The working medium was a 1 at.% Nd^{3+} ions and 0.01 at.% Cr ions doped Cr,Nd:YAG crystal thin plate (1.8 mm

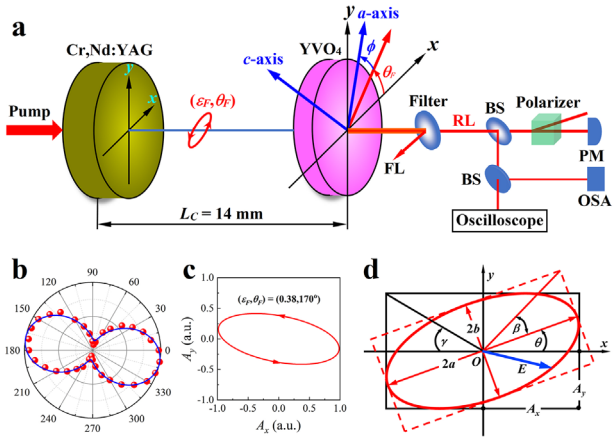

Figure 1. a) Schematic of experimental setup for manipulation of polarization states of elliptically polarized dual-wavelength passively Q-switched Raman laser by rotating *a*-cut YVO_4 crystal. θ_F is the azimuthal angle of the elliptically polarized fundamental laser. ϕ is the rotation angle of *a*-cut YVO_4 crystal with respect to the major axis of the elliptically polarized fundamental laser. *a*-axis and *c*-axis are crystalline orientations of *a*-cut YVO_4 crystal. *x*, *y* are the Cartesian coordinates. L_C is the cavity length, FL and RL are fundamental laser and Raman laser, BS is the beam splitter, PM and OSA are power meter and optical spectral analyzer. b) Transmitted power intensity of fundamental laser after passaging a linear polarizer. c) Polarization trajectory of the elliptically polarized fundamental laser. d) Elliptically polarized laser having components of amplitudes of A_x and A_y along the *x* and *y* axes, respectively. $\tan\gamma = A_y/A_x$. The major and minor axes of the ellipse are 2*a* and 2*b*; the ellipticity $\epsilon = b/a = \tan\beta$; the azimuthal angle is θ with respect to the *x* axis.

thick). The 1000–1200 nm high reflection (HR) and 808 nm antireflection (AR) were coated on one surface of the Cr,Nd:YAG crystal to serve as the rear cavity mirror. The other surface of Cr,Nd:YAG crystal was coated with 1064 nm AR to decrease the intracavity losses and 808 nm HR to increase the pump power absorption. A *a*-cut YVO_4 crystal (2 mm thick) was used as the Raman medium. One side facing the Cr,Nd:YAG crystal was coated with AR at 1000–1200 nm to reduce the Fresnel reflection loss, and the other side was coated with 1064 nm HR to act as output coupler. The total cavity length was 14 mm. The *a*-cut YVO_4 crystal was held by a copper clamp, which can be rotated around the axis of laser propagation direction. In our experiment, the *a*-cut YVO_4 crystal was rotated counterclockwise. The pump source is an 808 nm fiber coupled laser-diode (core diameter: 400 μm, numerical aperture: 0.22). Two spherical lenses (focal length: 8 mm) were used to collimate and focus the pump beam. The diameter of the focused pump beam footprint in the Cr,Nd:YAG crystal was about 150 μm. The polarization state of intracavity fundamental laser is elliptical polarization with an azimuthal angle of θ_F. ϕ is the rotation angle of *a*-axis of *a*-cut YVO_4 crystal with respect to the major axis of the elliptically polarized intracavity fundamental laser, when the intracavity fundamental laser propagates along [00$\bar{1}$] orientation of *a*-cut YVO_4 crystal. The laser was operated at room temperature without active cooling of active components.

A long-pass filter was used to separate Raman laser from total laser. An optical spectral analyzer (Anritsu, MS9740A) was used to analyze the laser spectra of the Cr,Nd:YAG/YVO_4 self-Q-switched Raman laser. The resolution of the optical spectral analyzer is 0.03 nm. The generated lasers were focused with

a lens (100 mm focal length), then coupled into a multimode fiber that connected the optical spectral analyzer. The average output powers of Raman laser were measured with a Thorlabs power meter. A Tektronix oscilloscope (MDO3104) was used to measure the pulse trains and pulse profile. The polarization states of the elliptically polarized Raman laser were measured by using a Glan-Thomson prism and a power meter (PM200).

In a Cartesian coordinate system, an arbitrary elliptically polarized laser beam propagating along z direction can be treated as superposition of two orthogonal linearly polarized beams along x- and y-axes with a phase difference. Therefore, an elliptically polarized laser beam can be expressed with superposition of two mutually orthogonal field components along x- and y-axes with a fixed phase difference between them, as shown in Figure 1d, and can be expressed with a vector $\boldsymbol{E}$ by[37]

$$E(t) = iA_x \cos(-\omega t) + jA_y \cos(-\omega t + \delta) \quad (1)$$

where A_x and A_y are the amplitudes of two orthogonal components along x and y axes, ω is the angular velocity, t is the elapsed time, $\boldsymbol{i}$ and $\boldsymbol{j}$ are the unit vectors along x-axis and y-axis.

From Figure 1d, we can see that the polarization trajectories of elliptically polarized lasers can be more clearly expressed by the major and minor axes, azimuthal angle, a, b, θ in the Cartesian coordinate system. More clearly, the SoP of the elliptically polarized laser can be expressed with ellipticity and azimuthal angle of an ellipse (ϵ,θ). The ellipticity, ϵ, is defined as $\epsilon = b/a$. The azimuth angle, θ, is the angle between the major axis a and the x-axis. The ellipticity and azimuthal angle of the elliptically polarized light can be obtained with following equations expressed with parameters A_x, A_y, and δ,

$$\tan(\gamma) = A_y/A_x, \epsilon = \tan(\beta) = b/a \quad (2)$$

$$\sin(2\beta) = \sin(2\gamma)\sin(\delta), \tan(2\theta) = \tan(2\gamma)\cos(\delta) \quad (3)$$

$$A_x^2 + A_y^2 = a^2 + b^2 \quad (4)$$

When an elliptically polarized laser passages through a linear polarizer, the transmitted power intensity as a function of rotation angle of the linear polarizer (φ), can be expressed as

$$I(\varphi) = \left(A_x \cos\varphi\right)^2 + \left(A_y \sin\varphi\right)^2 + 2A_x \cos\varphi \cdot A_y \sin\varphi \cdot \cos\delta \quad (5)$$

The parameter A_x, A_y, and δ of the elliptically polarized laser can be obtained by fitting measured transmitted power intensity as a function of φ. Thus, the SoP of the elliptically polarized laser can be determined with experimentally obtained parameters of A_x, A_y, and δ with Equations (2)–(4). Also, by using the experimentally obtained parameters of A_x, A_y, and δ, the polarization trajectory of the elliptically polarized laser can be recovered with Equation (1).

3. Results and Discussion

3.1. a-Cut YVO_4 Crystalline Orientation Dependent Laser Performance

The polarization state of the fundamental laser was determined by measuring the transmitted power intensity after passing through a linear polarizer when the Cr,Nd:YAG/YVO_4 self-Q-switched Raman laser oscillated in fundamental laser. As shown in Figure 1b, variation of the transmitted power intensity with rotation of linear polarizer is fitted well with Equation (5), which clearly provides that the fundamental laser is elliptical polarization with an azimuthal angle of 170°. The polarization state of the intracavity fundamental laser was doubly checked for the Cr,Nd:YAG/YVO_4 self-Q-switched Raman laser by rotating a-cut YVO_4 crystal and found that the residual fundamental laser was elliptically polarized with an azimuthal angle of about 170° independent on the rotation of a-cut YVO_4 crystal. The polarization trajectory of the left-handed elliptically polarized fundamental laser is given in Figure 1c. The elliptically polarized intracavity fundamental laser with a fixed azimuthal angle is maintained in the Cr,Nd:YAG/YVO_4 self-Q-switched Raman laser.

For simplicity, the a-axis of the a-cut YVO_4 crystal was aligned along the major axis of the elliptically polarized intracavity fundamental laser in the experiment for manipulating SoP of the elliptically polarized Raman laser. The effects of the crystalline orientation of a-cut YVO_4 crystal on the SoP of elliptically polarized Raman laser was studied by rotating a-cut YVO_4 crystal in counterclockwise direction. ϕ is the rotation angle of a-axis of a-cut YVO_4 crystal with respect to the major axis of the intracavity fundamental laser, $\phi = 0°$ indicates the a-axis of a-cut YVO_4 crystal parallel with major axis of the elliptically polarized intracavity fundamental laser, when the intracavity fundamental laser propagates along [00$\bar{1}$] of a-cut YVO_4 crystal.

3.1.1. Laser Spectra

When the incident pump power (P_{in}) reaches 0.52 W, the Cr,Nd:YAG/YVO_4 self-Q-switched Raman laser oscillates in fundamental laser around 1064 nm. The fundamental laser oscillated when P_{in} was less than 1.52 W. When the P_{in} reached over 1.52 W, the Raman lasers were excited to oscillate at 1166 and 1176 nm. The Raman shift lines of 816 and 890 cm^{-1} are utilized to generate 1166 and 1176 nm Raman lasers, respectively. **Figure 2**a shows some typical laser spectra at different rotation angles (rotation angle was selected from 90° to 135° for general case) of a-cut YVO_4 crystal for $P_{in} = 2.6$ W. The residual fundamental laser oscillates in two-longitudinal-mode around 1064.8 nm, while Raman lasers oscillate at 1166 and 1176.4 nm, respectively. As a-cut YVO_4 crystal rotates from 90° to 135°, the intensity of the residual fundamental laser decreases, while the overall intensity of two Raman lasers decreases with rotation angle when the rotation angle is less than 110° and then increases with further increasing of rotation angle of a-cut YVO_4 crystal. The Raman laser at 1176.4 nm oscillates in multilongitudinal-mode and mode number increases from 1 to 3 as rotation angle, ϕ, increases from 90° to 135°. Owing to mode competition and relative low Raman gain at 816 cm^{-1} compared to that at 890 cm^{-1}, the intensity of 1166 nm Raman laser converted with 816 cm^{-1} is weaker than that of 1176.4 nm Raman laser. Apparently, the longitudinal modes of 1166 nm Raman laser are less than those of 1176.4 nm Raman laser. Figure 2b shows the evolution of laser spectra of Cr,Nd:YAG/YVO_4 self-Q-switched Raman laser with increasing of incident pump power for rotation angle of 135° of a-cut YVO_4 crystal. The residual fundamental laser

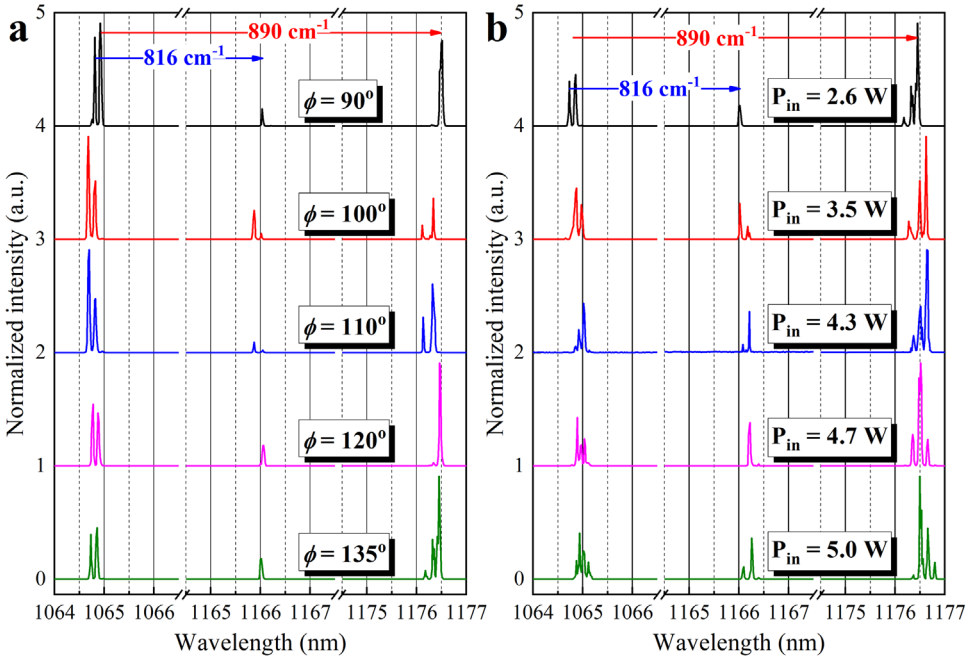

Figure 2. a) Evolution of laser spectra of Cr,Nd:YAG/YVO_4 self-Q-switched Raman laser with rotation angles of *a*-cut YVO_4 crystal, P_{in} = 2.6 W. b) Evolution of laser spectra of Cr,Nd:YAG/YVO_4 self-Q-switched Raman laser with P_{in}, rotation angle of *a*-cut YVO_4 crystal, ϕ = 135°.

oscillates in two longitudinal modes when P_{in} is lower than 3.6 W, then oscillates in three longitudinal modes at P_{in} = 4.3 and 4.7 W, four longitudinal modes oscillate at P_{in} = 5 W. The Raman laser at 1166 nm oscillates in single longitudinal mode at P_{in} = 2.6 W, the longitudinal mode number and intensity of 1166 nm Raman laser increases with P_{in}, three longitudinal modes oscillate at P_{in} = 5 W. The Raman laser at 1176.5 nm oscillates in three longitudinal modes at P_{in} = 2.6 W, three longitudinal modes oscillate until P_{in} reaches over 4.7 W, four longitudinal modes oscillate at P_{in} = 5 W. As shown in Figure 2b, the longitudinal mode number of residual fundamental laser and Raman lasers increases with P_{in} and the wavelengths of the residual fundamental laser and Raman laser shift to longer wavelength as increase in P_{in}. The increase of longitudinal modes and wavelength redshift are attributed to the thermal effect induced emission spectrum broadening of Nd:YAG crystal and Cr,Nd:YAG crystal.[38,39] The mode spacing of the fundamental laser was measured to be 0.08 nm while the mode spacing for the Raman lasers was measured to be about 0.15 nm. The free spectral range of a laser cavity can be expressed as $\Delta\lambda = \lambda^2/2L_C$, where λ is the laser wavelength and L_C is the optical cavity length. For Cr,Nd:YAG/YVO_4 self-Q-switched Raman laser studied here, $\Delta\lambda$ were calculated to be 0.075, 0.089, and 0.091 nm for 1064, 1166, and 1176 nm, respectively. The experimental mode spacing of the fundamental laser is in good agreement with free spectral range of fundamental laser, while the theoretically calculated mode spacing is smaller than those for Raman lasers. The wide mode spacing of Raman lasers is attributed to the tilted etalon effect of 2 mm thick YVO_4 crystal. Therefore, 1166/1176 nm dual-wavelength Raman laser has been obtained in the Cr,Nd:YAG/YVO_4 self-Q-switched Raman laser independent on the rotation angle of *a*-cut YVO_4 crystal and pump power when P_{in} is higher than the threshold pump power for Raman laser.

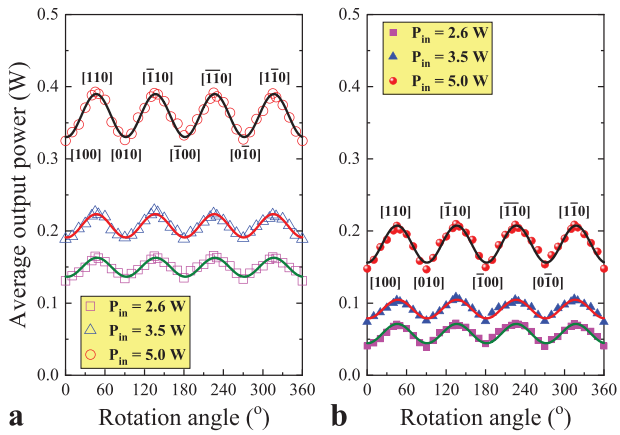

Figure 3. Dependence of average output power of a) total laser and b) Raman laser on rotation angles of *a*-cut YVO_4 crystal for three values of P_{in}s (2.6, 3.5, and 5 W). Solid lines are fitting of experimental data with a sine square function. The numbers in the brackets are some key crystalline orientations in the (001) plane of *a*-cut YVO_4 crystal.

3.1.2. Effect of Crystalline Orientation on Output Power

At different incident pump powers, the average output power of total laser and Raman laser were measured as *a*-cut YVO_4 crystal rotated. It can be seen from **Figure 3**, the average output power of total and Raman laser increases as the P_{in} increases, and there is concomitant observation of anisotropic behavior of average output power with *a*-cut YVO_4 crystal rotation angle. The output powers of total and Raman lasers reach a maximum when the rotation angle of *a*-cut YVO_4 crystal, ϕ, is 45°, 135°, 225°, and 315°, respectively. There are four sinusoidal modulation of the average output power of the total and Raman lasers in a full 360°

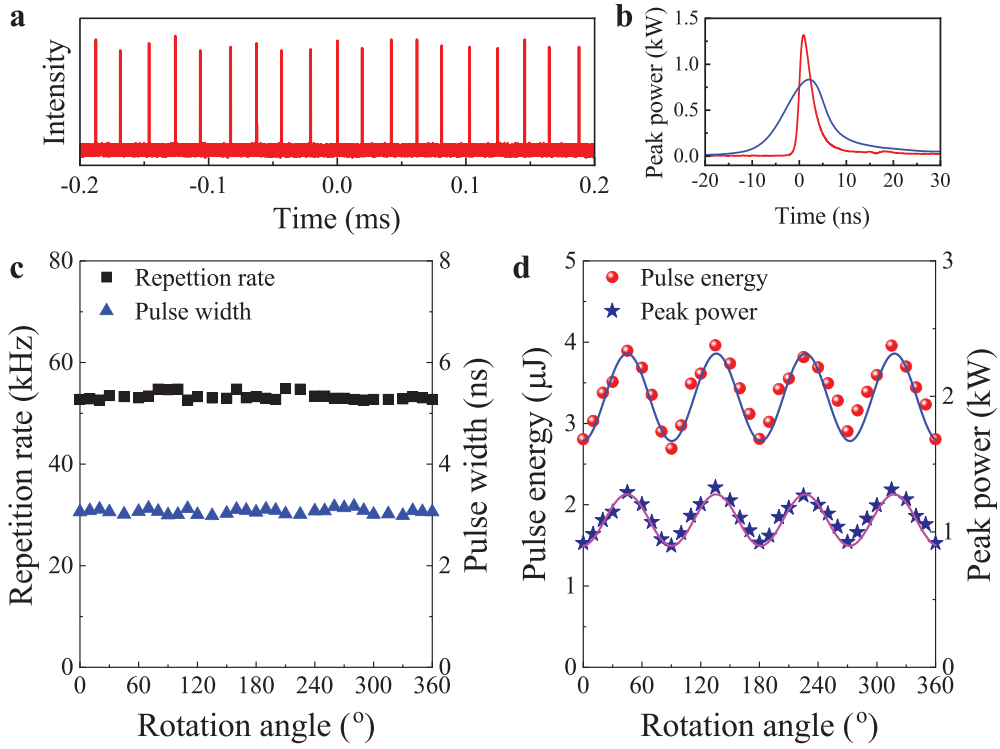

Figure 4. a) Raman laser pulse train and b) pulse profiles of Raman laser and residual fundamental laser at $P_{in} = 5$ W. c) Repetition rate and pulse width and d) pulse energy and peak power of Raman laser versus rotation angle of *a*-cut YVO_4 crystal at $P_{in} = 5$ W.

rotation. The four peaks of the average output power of total and Raman lasers are related to the four crystalline orientations of *a*-cut YVO_4 crystal, e.g., [110], [$\bar{1}$10], [$\bar{1}\bar{1}$0], [1$\bar{1}$0] in (001) plane. The four troughs of the average output power are related to four specified crystalline orientations, e.g., [100], [010], [$\bar{1}$00], [0$\bar{1}$0] in (001) plane. From Figure 2b, we can see that the modulation depth (maximum power at peak to minimum power at trough) of sinusoidal variation of the average output power of Raman laser decreases with P_{in}, e.g., 68–41 mW at $P_{in} = 2.6$ W, 108–70 mW at $P_{in} = 3.5$ W, 210–150 mW at $P_{in} = 5$ W. This is caused by the thermal induced depolarization effect of Cr,Nd:YAG crystal, which depends on the applied pump power. At available incident pump power of 5 W, the maximum average output power of Raman laser at 45°, 135°, 225°, and 315° is about 1.4 times of that at ϕ of 0°, 90°, 180°, and 270°. The maximum average output power of the total laser at 45°, 135°, 225°, and 315° is about 19% higher than that at 0°, 90°, 180°, and 270°. From Figure 3, we can conclude that the performance of passively Q-switched Raman laser strongly depends on the crystalline orientation of *a*-cut YVO_4 crystal. Especially, the average output power of the Raman laser at $P_{in} = 5$ W has been enhanced by over 40% by aligning crystalline orientations [110], [$\bar{1}$10], [$\bar{1}\bar{1}$0], [1$\bar{1}$0] along with the major axis of the elliptically polarized intracavity fundamental laser.

3.1.3. Effect of Crystalline Orientation on Laser Pulse Characteristics

The pulse trains and pulse profiles of the Raman laser at different rotation angles and P_{in}s were measured with an oscilloscope. The Raman laser pulses are generated from intracavity fundamental laser through stimulated Raman scattering effect, the Raman laser pulses are synchronized with fundamental laser pulses. A typical pulse train of Raman laser at $P_{in} = 5$ W is shown in **Figure 4**a. The fluctuation of the pulse intensity is less than 4% and the time jitter between pulse is less than 7%. The repetition rate is about 52 kHz. As shown in Figure 4b, the Raman laser pulse exhibits an asymmetric shape with a sharp rise and slow fall, which is a typical Raman laser pulse. The pulse width expressed with full width at half maximum (FWHM) is 3 ns and peak power is 1.3 kW. After conversion of Raman laser, the fundamental laser pulse is a profile with slow rise and sharp fall. The FWHM of the residual fundamental laser is 9.7 ns and peak power is 0.9 kW. The Raman laser pulse was narrowed during Raman conversion through stimulated Raman scattering effect.

The pulse energy of the Raman laser was obtained by dividing average output power with pulse repetition rate and peak power of the Raman laser was obtained by dividing pulse energy with pulse width. One typical example of Raman laser pulse characteristics as rotation of *a*-cut YVO_4 crystal was given at $P_{in} = 5$ W. The repetition rate and pulse width are kept nearly unchanged as the *a*-cut YVO_4 rotates in a full 360°, as shown in Figure 4c. The repetition rate and pulse width are 52 kHz and 3 ns. As shown in Figure 4d, the anisotropic behavior was observed for pulse energy and peak power. The pulse energy and peak power vary in a sinusoidal function as *a*-cut YVO_4 rotates. The pulse energy increases from 2.8 μJ at trough to 4 μJ at peak, while the peak power increases from 0.9 kW at trough to 1.3 kW at peak. There is about

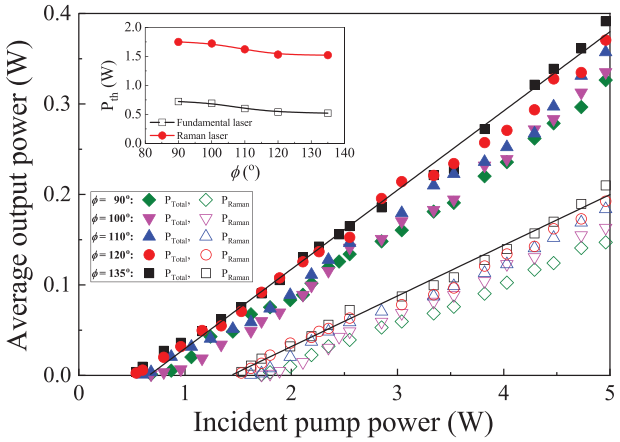

Figure 5. Average output power of the total laser and Raman laser versus P_{in} at different rotation angles of *a*-cut YVO_4 crystal. The lines are linear fit of average output power of total and Raman lasers at *a*-cut YVO_4 crystal rotation angle of 135°. Inset shows the variation of the threshold pump powers of fundamental and Raman lasers as a function of rotation angle of *a*-cut YVO_4 crystal.

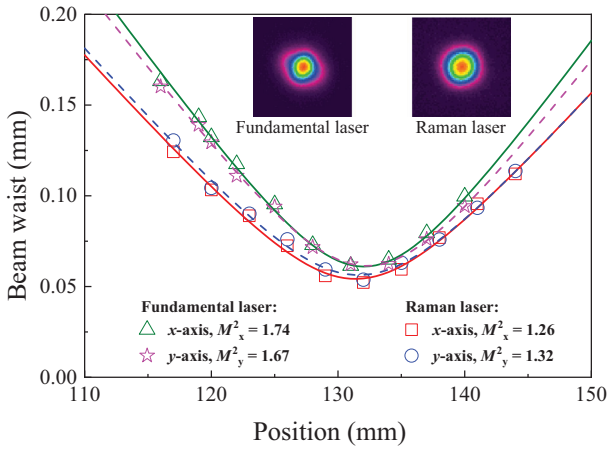

Figure 6. Position dependence of beam waist along beam propagation direction for fundamental and Raman lasers at P_{in} = 5 W. Solid lines are the theoretical fitting curves with beam propagation formula. Insets are the beam profiles of fundamental and Raman lasers.

40% increase of pulse energy and peak power from trough to the peak.

3.1.4. Effect of Pump Power on Output Power for Different Crystalline Orientations

For different rotations of *a*-cut YVO_4 crystal, the average output power of total and Raman lasers was measured as incident pump power increased. **Figure 5** shows the average output powers of total and Raman lasers as a function of P_{in} for five rotation angles from 90° to 135°. The threshold pump power of the fundamental and Raman laser decreases as *a*-cut YVO_4 crystal rotates from 90° to 135°, as shown in the inset in Figure 5. The lowest pump power thresholds for fundamental and Raman lasers were obtained at YVO_4 crystal rotation angle of 135°, and they are 0.52 and 1.52 W, respectively. The average output power of total and Raman lasers increases linearly with P_{in} for different rotation angles. The best laser performance was obtained at ϕ = 135°. The slope efficiencies of the total and Raman lasers were 8.7% and 5.6% for ϕ = 135°. When the available P_{in} was 5 W, the highest average output power of the total and Raman lasers were 391 and 210 mW, respectively. The corresponding optical efficiency of Raman laser was 4.2%. The average output power, slope efficiency, and optical efficiency of the total and Raman lasers decreases as YVO_4 crystal rotates from 135° to 90°. For both the total and Raman lasers, no output power saturation was found at current available pump power, therefore, the average output power of the Raman laser can be further scaled by applying high pump power.

The beam quality of the fundamental and Raman lasers was evaluated by measuring the beam radii at different positions along the beam propagation direction. The variation of the beam radii at different positions for fundamental and Raman lasers at P_{in} = 5 W was shown **Figure 6**. It is can be seen from the insets in Figure 6, the intensity profiles are TEM_{00} modes for both fundamental and Raman lasers. The Raman laser was a perfect Gaussian beam profile compared to the residual fundamental laser. The beam quality factors of the total and Raman laser were obtained by fitting the experimental data with beam propagation formula. The measured beam quality factors of the fundamental laser along horizontal and vertical direction are 1.74 and 1.67, respectively. The measured beam quality factors of the Raman laser along horizontal and vertical direction are 1.26 and 1.32, respectively. The beam quality of Raman laser is better than that of the fundamental laser, which further confirms that improvement of beam quality of Raman laser with the SRS effect. Therefore, near-diffraction-limited beam quality has been achieved in 1166/1176 dual-wavelength Raman laser.

3.2. *a*-Cut YVO_4 Crystalline Orientation Manipulated Elliptical Polarization

3.2.1. Crystalline Orientation Manipulated Elliptical Polarization

The polarization state of the Raman lasers was determined by measuring transmitted power intensity of the Raman laser after passing through a linear polarizer. When the *a*-axis of *a*-cut YVO_4 crystal is parallel to the major axis of the elliptically polarized intracavity fundamental laser, e.g., ϕ = 0°, variation of the transmitted power intensity with rotation of linear polarizer is shown in **Figure 7**a. Two maximum power intensities were obtained at 0° and 180°, while two nonzero minimum power intensities were obtained at 90° and 270°. The variation of transmitted power intensity with rotation of linear polarizer is fitted well with Equation (5), which clearly provides strong evidence that the Raman laser is elliptical polarization. When the *a*-cut YVO_4 crystal was rotated 45°, the elliptically polarized intracavity fundamental laser is aligned between *a*-axis and *c*-axis of *a*-cut YVO_4 crystal, the measured transmitted power intensity exhibits the same variation with rotation of linear polarizer as that at ϕ = 0°. The differences are that the orientation of the maximum transmitted power intensity rotates to 45° and minimum power intensity increases. When ϕ was further rotated to 90°, variation of the transmitted power intensity with rotation of linear polarizer is nearly identical to that at ϕ = 0°, however, the orientation of the maximum

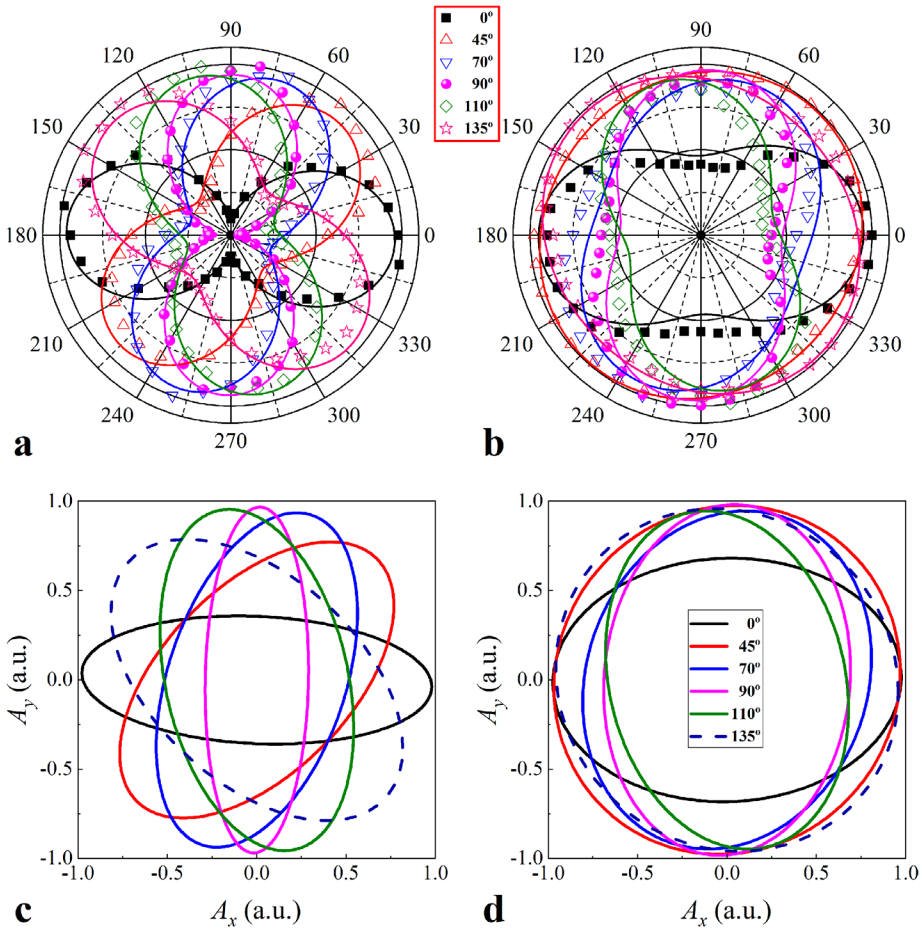

Figure 7. Measured transmitted power intensity after a linear polarizer of Raman laser at some typical rotation angles of *a*-cut YVO_4 crystal at a) $P_{in} = 3$ W and b) $P_{in} = 4.5$ W. c,d) Reconstructed polarization trajectories of the elliptically polarized Raman lasers at different rotation angles of *a*-cut YVO_4 crystal, corresponding to (a) and (b), respectively.

transmitted power intensity rotates to 90°. The transmitted power intensity with rotation of linear polarizer at $\phi = 70°$ is nearly identical to that at $\phi = 110°$, the minimum transmitted power intensity is larger than that at $\phi = 90°$ and smaller than that at $\phi = 45°$. The transmitted power intensity with rotation of the linear polarizer at $\phi = 135°$ is nearly identical to that at $\phi = 45°$, there are 90° difference between these two transmitted power intensities. Variation of the transmitted power intensity with rotation of linear polarizer at different rotation angles of *a*-cut YVO_4 crystal is fitted well with Equation (5), which indicates that the Raman lasers generated at different rotation angles of *a*-cut YVO_4 crystal are elliptical polarization, as shown in Figure 7a. The azimuthal angle of elliptical polarized Raman laser rotates coincidently as rotation of *a*-cut YVO_4 crystal. The elliptically polarized Raman laser tends to change and the minimum transmitted power intensity increases when the P_{in} is increased. At $P_{in} = 4.5$ W, as shown in Figure 7b, the azimuthal angle of the elliptically polarized Raman laser rotates as the same speed of the rotation of YVO_4 crystal. However, the minimum transmitted power intensity tends to increase comparable to the maximum power intensity at rotation angles of 45° and 135°, which tend to be circular polarization. The normalized minimum transmitted power intensity at rotation angles of 0° and 90° increases as P_{in} increases, as shown in Figure 7b. Anisotropic emission properties of *a*-cut YVO_4 crystal are responsible for the elliptically polarized Raman laser oscillation under elliptically polarized intracavity fundamental laser pumping. The enlarge of ellipticity of elliptically polarized Raman laser with pump power is attributed to the depolarization effect of *a*-cut YVO_4 crystal.

Based on the experimentally measured transmitted power intensity as a function of rotation angle of linear polarizer for different crystalline orientations of *a*-cut YVO_4 crystal at different pump powers (Figure 7a,b), the parameters of A_x, A_y, and δ were obtained by fitting the experimental data with Equation (5). With fitted parameters of A_x, A_y, and δ of elliptically polarized lasers at different rotation angles of *a*-cut YVO_4 crystal, the corresponding shape (ϵ) and orientation (θ) of the elliptically polarized lasers were determined.

Therefore, the experimentally obtained elliptically polarized lasers at different rotation angles of *a*-cut YVO_4 crystal were plotted with Equation (1) by using experimentally fitted parameters of A_x, A_y, and δ. The reconstructed polarization trajectories of the elliptically polarized Raman lasers at different rotation angles of *a*-cut YVO_4 crystal and different pump powers are shown in Figure 7c,d. From Figure 7c,d, we can clearly see that the shape and orientation of elliptically polarized Raman laser

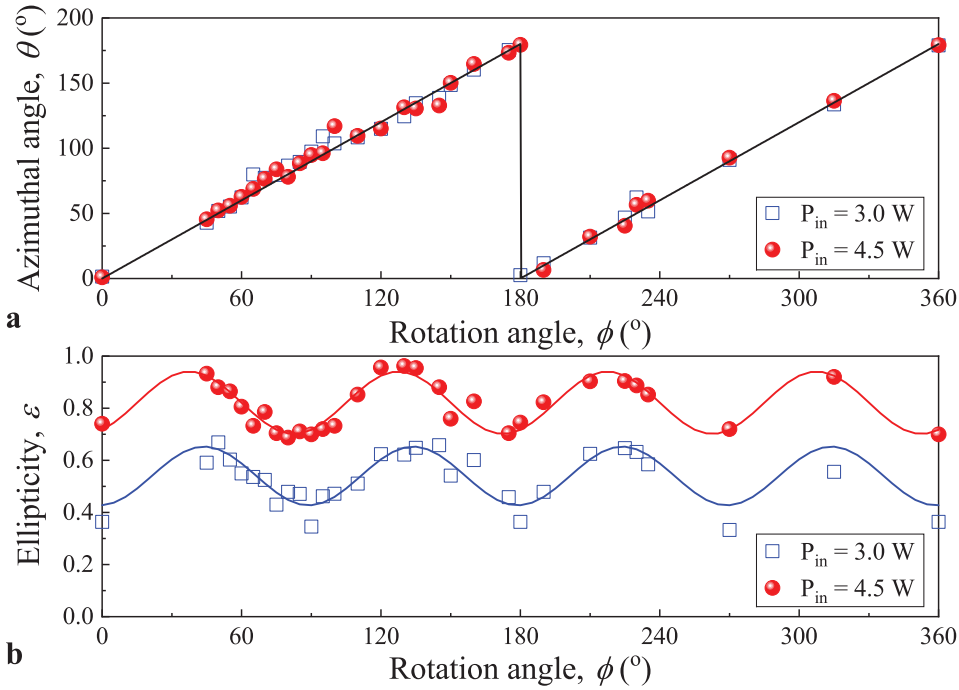

Figure 8. a) Azimuthal angle (θ) and b) ellipticity (ϵ) of the experimentally generated elliptically polarized Raman laser as rotation of *a*-cut YVO_4 crystal at P_{in} = 3 W and P_{in} = 4.5 W. The solid lines are the fitting curves with Equations (6) and (7), respectively.

change with rotation angle of *a*-cut YVO_4 crystal and pump power. As shown in Figure 7c, at P_{in} = 3 W, the ellipticity of elliptically polarized laser decreases as YVO_4 crystal rotates from 45° to 90° and then increases as YVO_4 crystal further rotates from 90° to 135°. Meanwhile, the azimuthal angle or orientation of the major axis rotates in the same speed as rotation of YVO_4 crystal. At P_{in} = 4.5 W, the ellipticity of elliptically polarized laser increases for different rotation angles of *a*-cut YVO_4 crystal, while the azimuthal angle of the elliptically polarized laser rotates in the same speed as the rotation of *a*-cut YVO_4 crystal. Especially, the near circularly polarized lasers are obtained at rotation angles of 45° and 135°, as shown in Figure 7d. Therefore, elliptically polarized Raman laser with flexible ellipticity and azimuthal angle has been obtained in the self-Q-switched Raman laser by rotating *a*-cut YVO_4 crystal and adjusting pump power.

Figure 8 shows the azimuthal angle and the ellipticity of the experimentally obtained elliptically polarized Raman laser at different rotation angles of *a*-cut YVO_4 crystal. From Figure 8a, we can see that the azimuthal angle of the elliptically polarized laser at different pump powers increases linearly with rotation angle of *a*-cut YVO_4 crystal. Owing to the fourfold symmetry of *a*-cut YVO_4 crystal, the azimuthal angle of the elliptically polarized Raman laser shifts to 0° when the rotation angle of *a*-cut YVO_4 crystal reaches to 180° and then increases linearly with rotation angle of *a*-cut YVO_4 crystal. The variation of the azimuthal angle of the elliptically polarized Raman laser with rotation angle of *a*-cut YVO_4 crystal can be expressed as follows

$$\theta = \begin{cases} \phi, 0 \le \phi \le \pi \\ \phi - \pi, \pi < \phi \le 2\pi \end{cases} \quad (6)$$

As shown in Figure 8b, the ellipticity of the elliptically polarized Raman laser exhibits four peaks and four troughs as *a*-cut YVO_4 crystal rotates in a full 360°. The ellipticity of the elliptically polarized Raman laser reaches maximum when the rotation angle of *a*-cut YVO_4 crystal, ϕ, is 45°, 135°, 225°, and 315°, respectively. The variation of the ellipticity with rotation angle of *a*-cut YVO_4 crystal at different pump powers is fitted well with sine square function. The ellipticity of the elliptically polarized Raman laser increases as pump power increases for a certain rotation angle of *a*-cut YVO_4 crystal. The variation of the ellipticity of the elliptically polarized laser as a function of rotation angle of *a*-cut YVO_4 crystal and pump power can be expressed as

$$\epsilon(P,\phi) = \left[-4.02 + 4.81\left(1 - e^{\frac{-P}{1.14}}\right)\right] + \left[-0.79 + 1.04\left(1 - e^{\frac{-P}{0.75}}\right)\right]\sin^2(2\phi) \quad (7)$$

where P and ϕ are the incident pump power and rotation angle of *a*-cut YVO_4 crystal.

3.2.2. Mechanism of Manipulation of Elliptical Polarization with Crystalline Orientation

In order to qualitatively illustrate the *a*-cut YVO_4 crystalline orientation dependent anisotropic behaviors observed in Cr,Nd:YAG/YVO_4 self-Q-switched Raman laser, we assume the fast-axis of the elliptically polarized intracavity fundamental laser is assigned parallel to *x*-axis in Cartesian coordinate system, ϕ is the angle between the crystallographic axis [100] of *a*-cut YVO_4 crystal and *x*-axis or the fast-axis of the elliptically polarized fundamental laser. **Figure 9**a shows the anisotropic crystalline structure of

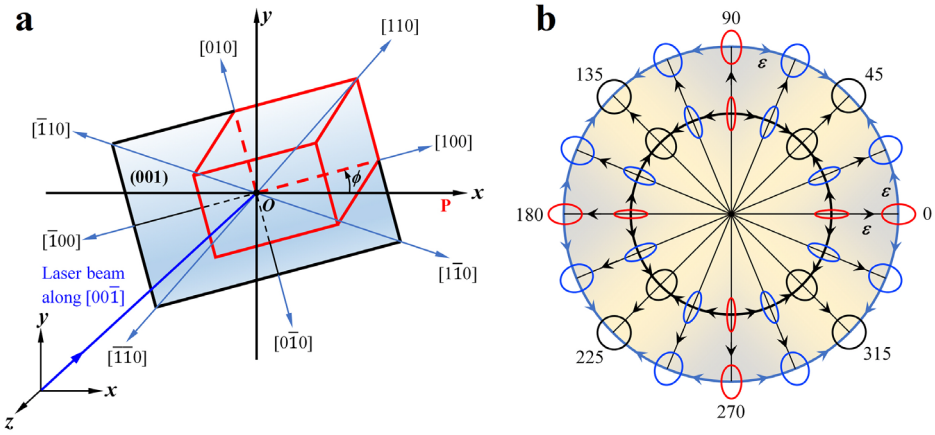

Figure 9. a) Crystalline orientations in (001) plane of *a*-cut YVO_4 crystal. *a*-axis and *c*-axis of *a*-cut YVO_4 crystal are aligned at an angle of ϕ with respect to the *x*-axis and *y*-axis, respectively. The fundamental laser propagates along [00$\bar{1}$] direction. *P* represents the major axis of the elliptically polarized fundamental laser. ϕ is the angle between *x*-axis and the major axis of the elliptically polarized fundamental laser beam, $\phi = 0°$ indicates that the *a*-axis of *a*-cut YVO_4 crystal is parallel to major axis of the elliptically polarized fundamental laser. b) Elliptical polarization states of Cr,Nd:YAG/YVO_4 self-Q-switched Raman laser at different rotation angles between *a*-axis of *a*-cut YVO_4 crystal and the major axis of the elliptically polarized fundamental laser. The applied pump power is illustrated with two large circles. ϵ is the ellipticity of elliptically polarized laser, which is defined as ratio of the minor axis and the major axis. The arrows indicate the increase of ellipticity, ϵ.

a-cut YVO_4 crystal and some special crystalline orientations in (001) plane with respect to the fundamental laser beam propagation direction. In Cartesian coordinate system, crystallographic direction [001] is assigned along *z*-axis, while crystallographic directions [100], [010] are aligned an angle of ϕ with respect to *x*-, *y*-axes, respectively. In (001) plane, four orientations [100], [010], [$\bar{1}$00], and [0$\bar{1}$0] are indicated. Other four crystalline orientations such as [110], [$\bar{1}$10], [$\bar{1}\bar{1}$0], and [1$\bar{1}$0] are also indicated. These eight crystalline orientations have been chosen to illustrate the observed anisotropic behavior of the Raman laser.

In the Cr,Nd:YAG/YVO_4 Raman laser, Raman laser is generated through SRS effect of *a*-cut YVO_4 crystal under intracavity fundamental laser pumping. For the fundamental laser with elliptical polarization, the laser electric field is expressed with an amplitude $|\boldsymbol{E}|$, ellipticity ϵ_F, azimuthal angle θ_F

$$E(t) = \frac{|E|}{\sqrt{1+\epsilon_F^2}} \begin{bmatrix} \cos(\theta_F) & -\sin(\theta_F) \\ \sin(\theta_F) & \cos(\theta_F) \end{bmatrix} \begin{bmatrix} 1 \\ i\epsilon_F \end{bmatrix} e^{i\omega t} \tag{8}$$

To illustrate the effect of crystalline orientation of *a*-cut YVO_4 crystal on the polarization of elliptically polarized Raman laser generated in the Cr,Nd:YAG/YVO_4 self-Q-switched Raman laser, the fast-axis components of the elliptically polarized fundamental laser is assumed to along *x*-axis. Therefore, in the Cr,Nd:YAG/YVO_4 self-Q-switched Raman laser, when the elliptically polarized fundamental laser passages through the *a*-cut YVO_4 birefringent crystal, the generated elliptically polarized Raman laser is expressed in terms of components parallel and perpendicular to the optic axis of the *a*-cut YVO_4 crystal

$$E(t) = \begin{bmatrix} \cos(\theta) & \sin(\theta) \\ \sin(\theta) & -\cos(\theta) \end{bmatrix} \begin{bmatrix} 1 & 0 \\ 0 & e^{i\delta} \end{bmatrix} \begin{bmatrix} \cos(\theta) & \sin(\theta) \\ \sin(\theta) & -\cos(\theta) \end{bmatrix} \times \frac{|E|}{\sqrt{1+\epsilon_F^2}} \begin{bmatrix} 1 \\ i\epsilon_F \end{bmatrix} e^{i\omega t} \tag{9}$$

where θ is the angle between the fast axis of the fundamental laser and the optic axis of the *a*-cut YVO_4 birefringent crystal, here $\theta = \phi$. $\delta = kd(n_e - n_o)$ is the phase difference, k is the free-space wavenumber, d is the thickness of the birefringence crystal, n_e and n_o are the refractive indices of the birefringent crystal experienced by extraordinary and ordinary rays, respectively.

From Equation (9), we can clearly see that the contributions from two components of the elliptically polarized fundamental laser strongly depend on the angle between fast axis of the elliptically polarized fundamental laser and *a*-axis of *a*-cut YVO_4 crystal. When the fast axis of the elliptically polarized fundamental laser is exactly parallel with one particular crystallographic orientation in (001) plane, e.g., [100], elliptically polarized Raman laser is obtained because the perfect overlap is achieved between electric fields of elliptically polarized fundamental laser and the anisotropic Raman gain medium. If the [100] crystallographic orientation of *a*-cut YVO_4 crystal is not exactly parallel with the fast axis of the elliptically polarized intracavity fundamental laser, partial overlap with another crystallographic orientation will compensate. Therefore, elliptically polarized Raman laser is obtained since two partial electrical fields from orthogonal orientations of YVO_4 crystal contribute to the polarization state of elliptically polarized Raman laser. Especially, when the crystalline orientation of *a*-cut YVO_4 crystal, [1$\bar{1}$0] is exactly parallel with the fast axis of the fundamental laser, e.g., $\phi = 45°$, the contribution from two orthogonal orientations [100] and [0$\bar{1}$0] makes the Raman laser oscillate in elliptical polarization with large ellipticity at low pump power or circular polarization at high pump power. At high pump power level, owing to the thermal effect induced depolarization, the elliptical polarization state of Raman laser is changed to elliptical polarization with large ellipticity or even a circular polarization state. The elliptical polarization state of Raman laser at four specified crystalline orientations ([100], [010], [$\bar{1}$00] and [0$\bar{1}$0]) is changed to elliptical polarization state with increased ellipticity.

Polarization state of elliptically polarized dual-wavelength Raman laser can be manipulated by aligning *a*-cut YVO_4 crystal

orientation along with the fast axis of the elliptically polarized fundamental laser in a passively Q-switched Raman laser. The ellipticity of the elliptically polarized Raman laser can be flexible controlled by adjusting the crystalline orientation of *a*-cut YVO_4 crystal and incident pump power. Circularly polarized Raman laser can be obtained by aligning the fast axis of the elliptically polarized intracavity fundamental laser along [110] direction of *a*-cut YVO_4 crystal at high pump power levels. The elliptically polarized Raman laser with desired ellipticity and azimuthal angle can be easily achieved by aligning *a*-cut YVO_4 crystalline orientation along the major axis of the elliptically polarized intracavity fundamental laser or adjusting the applied pump power in a passively Q-switched Raman laser.

Figure 9b depicts possible anisotropic variation of the polarization states of elliptically polarized Cr,Nd:YAG/YVO_4 self-Q-switched Raman laser with rotation angles of *a*-cut YVO_4 crystal and pump power. At low pump power level, elliptically polarized lasers with small ellipticity were obtained at four rotation angles of *a*-cut YVO_4 crystal (0°, 90°, 180°, and 270°). The ellipticity of elliptically polarized Raman laser increases as rotation angle (ϕ) of *a*-cut YVO_4 crystal increases. For a certain pump power, elliptically polarized laser with a large ϵ is achieved at rotation angle of 45°. Further increasing rotation angle from 45° to 90°, the ϵ decreases, which means the elliptical polarization change in ellipticity and azimuthal angle. The similar change of elliptical polarization states with varying ϵ, and azimuthal angle was also observed as *a*-cut YVO_4 rotates from 90° to 180°, 180° to 270°, and 270° to 360°, respectively. When the pump power further increases, the circular polarization state is observed at rotation angles of 45°, 135°, 225°, and 315°, while the ellipticity increases for the elliptically polarized Raman laser at rotation angles of 0°, 90°, 180°, and 270°. The ellipticity of the elliptical polarization states at other rotation angles are also increases as pump power increases.

Furthermore, the high peak power sub-nanosecond dual-wavelength Raman laser with desired elliptical polarization can be achieved by further shortening the cavity length of passively Q-switched Raman laser. When *a*-cut YVO_4 crystal with specified crystalline orientation was attached Cr,Nd:YAG crystal to form passively Q-switched Raman microchip laser, the intracavity losses such as diffraction loss were further decreased, the intracavity fundamental laser intensity was further enhanced by shortening the cavity length, which was favorable for efficient Raman laser conversion from the fundamental laser by utilizing different Raman shift lines of *a*-cut YVO_4 crystal. Therefore, highly efficient, high peak power microchip Raman laser with desired elliptical polarization is ready to be developed. The ellipticity and azimuthal angle of the elliptically polarized high peak power Raman laser is controlled depending on the applications.

4. Conclusion

In summary, high beam quality, high peak power 1166/1176 nm dual-wavelength Raman laser with elliptical polarization has been demonstrated in a Cr,Nd:YAG/YVO_4 self-Q-switched Raman laser converted from 1064 nm fundamental laser with 816 and 890 cm^{-1} Raman shift lines. Elliptical polarization with controllable ellipticity and azimuthal angle has been achieved by aligning different crystalline orientation of the *a*-cut YVO_4 crystal along the major axis of the elliptically polarized fundamental laser and adjusting pump power. The ellipticity of the elliptically polarized Raman laser varies in a sine square modulation with rotation of *a*-cut YVO_4 crystal. The azimuthal angle of the elliptically polarized Raman laser changes in the same direction and speed with rotation of *a*-cut YVO_4 crystal. Anisotropic behavior of sinusoidal modulation of output power, pulse energy, peak power has been observed as rotation of *a*-cut YVO_4 crystal. There is about 40% disparity between trough and peak for Raman laser. Enhanced performance of passively Q-switched Raman laser at [110] crystalline orientation of *a*-cut YVO_4 crystal aligning along the major axis of the elliptically polarized intracavity fundamental laser is attributed to overall contribution from the electrical fields of both orientations along [100] and [010] of *a*-cut YVO_4 crystal. This work provides a solid experimental foundation and simple method for manipulating polarization state of elliptically polarized Raman laser generated in an efficient passively Q-switched Raman laser with selecting suitable crystalline orientations of anisotropic Raman gain medium.

Acknowledgements

This work was supported by the National Natural Science Foundation of China (61275143 and 61475130) and the Program for New Century Excellent Talents in University (NCET-09-0669).

Conflict of Interest

The authors declare no conflict of interest.

Author Contributions

Y.A. and H.Y. designed the Cr,Nd:YAG/YVO_4 self-Q-switched Raman laser, and carried out measurements. Y.A. also analyzed the results and wrote the paper. B.L. and J.B. performed the reconstruction of elliptical trajectories of elliptically polarized Cr,Nd:YAG/YVO_4 self-Q-switched Raman laser. J.D. led the project and proposed the idea, analyzed the results, and wrote the paper. All authors contributed to the final paper.

Data Availability Statement

Research data are not shared.

Keywords

crystalline orientation, elliptical polarization, passively Q-switched lasers, polarization manipulation, Raman lasers

Received: February 17, 2021
Revised: April 9, 2021
Published online: May 13, 2021

[1] G. C. Rodrigues, J. R. Duflou, *J. Mater. Process. Technol.* **2019**, *264*, 448.
[2] M. M. Hossain, H. Sakai, *J. Chem. Phys.* **2020**, *153*, 104102.
[3] J. S. Liu, Q. Y. Cheng, D. G. Yue, X. C. Zhou, Q. T. Meng, *Chin. Opt. Lett.* **2018**, *16*, 103201.

[4] M. E. J. Friese, T. A. Nieminen, N. R. Heckenberg, H. Rubinsztein-Dunlop, *Nature* **1998**, *394*, 348.
[5] N. Yoshikawa, T. Tamaya, K. Tanaka, *Science* **2017**, *356*, 736.
[6] S. Rostami, M. Chini, K. Lim, J. P. Palastro, M. Durand, J. C. Diels, L. Arissian, M. Baudelet, M. Richardson, *Sci. Rep.* **2016**, *6*, 20363.
[7] Y. S. You, T. I. Oh, K. Y. Kim, *Opt. Lett.* **2013**, *38*, 1034.
[8] Q. Z. Rong, X. G. Qiao, H. Z. Yang, Z. H. Shao, R. H. Wang, D. Su, *IEEE J. Sel. Top. Quantum Electron.* **2014**, *20*, 1100605.
[9] H. Xu, S. Yuan, Z. R. Guo, Q. S. Zhang, Y. Y. Ma, Q. Hao, K. Huang, M. Li, Y. Nie, H. P. Zeng, *Appl. Sci. (Basel , Switz.)* **2020**, *10*, 669.
[10] H. H. Yu, J. H. Liu, H. J. Zhang, A. A. Kaminskii, Z. P. Wang, J. Y. Wang, *Laser Photonics Rev.* **2014**, *8*, 847.
[11] X. L. Meng, L. Zhu, H. J. Zhang, C. Q. Wang, Y. T. Chow, M. K. Lu, *J. Cryst. Growth* **1999**, *200*, 199.
[12] V. E. Kisel, A. E. Troshin, N. A. Tolstik, V. G. Shcherbitsky, N. V. Kuleshov, V. N. Matrosov, T. A. Matrosova, M. I. Kupchenko, *Appl. Phys. B: Lasers Opt.* **2005**, *80*, 471.
[13] A. A. Kaminskii, K. Ueda, H. J. Eichler, Y. Kuwano, H. Kouta, S. N. Bagaev, T. H. Chyba, J. C. Barnes, G. M. A. Gad, T. Murai, J. R. Lu, *Opt. Commun.* **2001**, *194*, 201.
[14] H. B. Shen, Q. P. Wang, X. Y. Zhang, Z. J. Liu, F. Bai, Z. H. Cong, X. H. Chen, Z. G. Wu, W. T. Wang, L. Gao, W. X. Lan, *Opt. Lett.* **2012**, *37*, 4113.
[15] Y. F. Chen, *Opt. Lett.* **2004**, *29*, 1915.
[16] Y. F. Chen, *Opt. Lett.* **2004**, *29*, 1251.
[17] T. Healy, F. C. G. Gunning, A. D. Ellis, *Opt. Express* **2007**, *15*, 2981.
[18] Y. He, B. J. Orr, *Appl. Phys. B: Lasers Opt.* **2002**, *75*, 267.
[19] F. Weigl, *Appl. Opt.* **1971**, *10*, 1083.
[20] R. W. Farley, P. D. Dao, *Appl. Opt.* **1995**, *34*, 4269.
[21] K. Zhong, C. L. Sun, J. Q. Yao, D. G. Xu, X. Y. Xie, X. L. Cao, Q. L. Zhang, J. Q. Luo, D. L. Sun, S. T. Yin, *IEEE J. Quantum Electron.* **2013**, *49*, 375.
[22] C. B. Reid, E. Pickwell-MacPherson, J. G. Laufer, A. P. Gibson, J. C. Hebden, V. P. Wallace, *Phys. Med. Biol.* **2010**, *55*, 4825.
[23] Y. F. Chen, *Opt. Lett.* **2004**, *29*, 2172.
[24] G. Shayeganrad, *Opt. Commun.* **2013**, *292*, 131.
[25] J. Suda, *Spectrochim. Acta, Part A* **2018**, *192*, 333.
[26] K. W. Su, Y. T. Chang, Y. F. Chen, *Appl. Phys. B: Lasers Opt.* **2007**, *88*, 47.
[27] X. J. Wang, X. L. Wang, Z. F. Zheng, X. H. Qiao, J. Dong, *Appl. Opt.* **2018**, *57*, 3198.
[28] F. J. Zhuang, Z. Y. Lin, S. Q. Zhu, *Opt. Mater.* **2016**, *60*, 290.
[29] X. L. Wang, J. Dong, X. J. Wang, J. Xu, K. Ueda, A. A. Kaminskii, *Opt. Lett.* **2016**, *41*, 3559.
[30] J. Dong, A. Shirakawa, K. Ueda, *Appl. Phys. Lett.* **2008**, *93*, 101105.
[31] H. Eilers, K. R. Hoffman, W. M. Dennis, S. M. Jacobsen, W. M. Yen, *Appl. Phys. Lett.* **1992**, *61*, 2958.
[32] J. Dong, P. Z. Deng, Y. T. Lu, Y. H. Zhang, Y. P. Liu, J. Xu, W. Chen, *Opt. Lett.* **2000**, *25*, 1101.
[33] J. Dong, P. Z. Deng, M. Bass, *Opt. Laser Technol.* **2002**, *34*, 589.
[34] J. Dong, K. Ueda, *Appl. Phys. Lett.* **2005**, *87*, 151102.
[35] J. Dong, P. Z. Deng, Y. P. Liu, Y. H. Zhang, G. S. Huang, F. X. Gan, *Chin. Phys. Lett.* **2002**, *19*, 208.
[36] J. Dong, A. Shirakawa, S. Huang, Y. Feng, K. Takaichi, M. Musha, K. Ueda, A. A. Kaminskii, *Laser Phys. Lett.* **2005**, *2*, 387.
[37] P. S. Theocaris, *Appl. Opt.* **1979**, *18*, 4017.
[38] J. Dong, A. Rapaport, M. Bass, F. Szipocs, K. Ueda, *Phys. Status Solidi A* **2005**, *202*, 2565.
[39] S. Z. Zhao, A. Rapaport, J. Dong, B. Chen, P. Z. Deng, M. Bass, *Opt. Laser Technol.* **2006**, *38*, 645.